

AIYONG CUI¹, JIALEI ZHAO^{2*}, BORONG SHAN¹, HAODONG LIU¹,
WEIQI SUN¹, FANGYOU HU³, HUAKAI WEI¹

HIGH-FREQUENCY ULTRASONIC IMPACT TREATMENT EFFECT ON FATIGUE PROPERTIES OF TC4 TITANIUM ALLOY LASER WIRE FILLING-WELDED JOINTS

This study aimed to improve the fatigue properties of TC4 titanium alloy laser-filled wire welded joints. To this end, the high-frequency ultrasonic impact technology (UIT) was used to implement post-weld impact treatment on the welded part. Nondestructive testing of the phase composition, microstructure, microhardness, static and cyclic tensile properties, and fracture morphology before and after UIT were conducted and comparatively analyzed. The results show that the high-frequency UIT refines surface grains without affecting the weld phase composition, which is still dominated by the martensitic α' phase and does not form the ω phase. Due to plastic slip-induced strain-hardening, the microhardness of the weld surface layer is about 12% higher than before the UIT and about 40% higher than that of the base metal. Before UIT, long and thick cracks at static tensile fracture extend on the specimen surface; after UIT, the static tensile fracture surface is fine and smooth, and tiny cracks expand in the interior. The fatigue limit of the laser wire filling welding (LFW) in the TC4 titanium alloy joint increased by about 29.4% after UIT. After high-frequency ultrasonic impact, cracks expand in the joint; the fatigue band spacing becomes smaller, and dimples are denser and deeper, while the fatigue limit load increases, effectively improving the fatigue resistance of the TC4 titanium alloy laser wire-filling welded joint.

Keywords: High-frequency ultrasonic impact; Laser wire filling welding; Microhardness; Fatigue life; Fracture morphology

1. Introduction

TC4 titanium alloys combine excellent strength and corrosion resistance with good high- and low-temperature performance. With the development of the modern aviation industry, TC4 titanium alloys have found extensive applications in manufacturing tail nozzles, aircraft engines, heat shields, and accessory gearboxes [1-3]. However, TC4 titanium alloys are prone to cracking under the joint influence of impact vibration, alternating high- and low-temperature loads, and marine corrosion in an adverse service environment [4,5], seriously endangering flight safety. TC4 titanium alloy is widely known for its solderability [6]. Residual thermal stresses are considered inevitable in TC4 titanium alloy due to ultra-high temperature gradient, non-equilibrium rapid melting, and heterogeneous thermodynamic effects, which are the main factors shortening the service life of welded parts [7-9].

The damage mechanism of titanium alloy mainly includes three kinds: fatigue damage, corrosion damage and thermal dam-

age. Among them, fatigue damage is the most common form of titanium alloy damage, usually under the action of cyclic load will gradually appear micro-cracks, and eventually lead to material failure. To prolong the fatigue life of titanium alloy, the stress concentration can be reduced by forming the weld fillet transition section by impact and the behavior under different load conditions can be adopted. Li et al. [10,11] studied the influence of high-frequency ultrasonic vibration on the performance of LFW of TC2 titanium alloys and 5A06 aluminum alloys. Dekhtyar [12] investigated the influence of UIT on high-strength steel and TC4 titanium alloy laser welding performance. However, more research needs to be conducted concerning wide cracks in TC4 titanium alloys and the effects of UIT following LFW on fatigue properties. The present study focused on the reinforcement offered by UIT on the welded joint created by laser wire-filling welding LFW in the TC4 titanium alloy. The phase composition, microstructures, microscopic hardness, and fatigue properties before and after UIT were compared to providing theoretical and practical support for UIT-based engineering applications.

¹ QINGDAO CAMPUS OF NAVAL AVIATION UNIVERSITY, QINGDAO, 266041, CHINA

² LIAONING UNIVERSITY OF TECHNOLOGY, SCHOOL OF MECHANICAL ENGINEERING, JINZHOU, 121001, CHINA

³ WUXI ZHONGKE JINYAN LASER GAS TURBINE PARTS CO, LTD., WUXI, 214400, CHINA

* Corresponding author: 18791068136@163.com



2. Material and methods

The materials under study were TC4 alloy sheets with dimensions of 70 mm×45 mm×1.5 mm and TC4 solder wires with dimensions of 1.0 mm in diameter. Their chemical compositions are listed in TABLE 1.

TABLE 1

Chemical composition of TC4 titanium alloy sheet/solder wires
(%, mass fraction)

Al	V	Fe	C	N	H	O	Ti
6.32	4.15	≤0.05	≤0.08	≤0.05	≤0.013	≤0.2	Rest

The TC4 titanium alloy test plate and welding wire were mechanically treated and cleaned before welding; the surface oxidation layer and oil were removed, washed, and dried with absolute ethyl alcohol. The LFWW parameters were as follows: power of the fiber laser 800 W, welding travel speed 800 mm/min-1000 mm/min, filler wire feed rate of 240-280 cm/min, positive defocusing amount of 0.2 mm, air flow rate of 7-10 L/min, and high-purity argon gas used to protect the front and back sides. A 120 W ultrasound impact power and a 20 kHz frequency were applied for UIT. Two pins of 1.5 mm in diameter were used; the UIT impact was targeted at the weld part of the quasi-sample, being nearly perpendicular to the weld. Certain pressure was applied during the impact process to ensure a good impact effect, with the impact area twice exceeding the weld area, and to repeat the impact at a certain speed. During the impact process, the gun swang at a certain angle perpendicular to the weld so that the joint part of the weld zone (WZ) and the base material zone (BM) could get a smoother transition shape. A 1.5 mm-thin specimen was easy to deform. After multiple impacts, there was a gap between the specimen and the backing plate. The specimen was turned over with an amplitude of 25 μm and 100% weld coverage. UIT was repeated five times, ensuring the specimen was not deformed. The UIT schematic diagram is shown in Fig. 1.

The base metal and weld metal metallographic structure and fracture morphology were observed using an S-3400 N scanning electron microscope (SEM). Their cross-sectional views

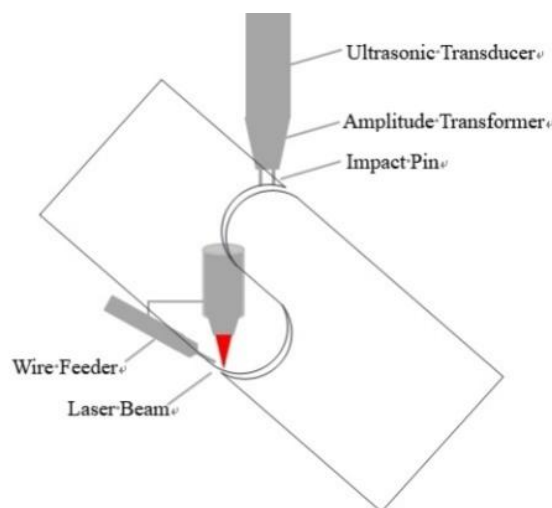


Fig. 1. Schematic diagram of LFWW joint after UIT

are shown in Fig. 2(a) and 2(b). Phase analysis was performed using a Malvern Panalytical-DY2495 X-ray diffractometer with Cu test radiation source, wavelength of 1.54, X-ray tube voltage of 40 kV, and current of 30 mA. The fixed peak method was Lorentz fitting, with a diffraction angle range of 0~180°. Metallographic samples were prepared after grinding, polishing, and etching before and after strengthening, and their microstructure morphology was observed. Polished samples were etched with a corrosive ratio of HF:HNO₃: H₂O = 20:10:85 (volume ratio) for about 1 min, quickly cleaned with anhydrous ethanol, and finally dried with a hair dryer. A Bx53MRF-S optical microscope (OM) observed the microstructure of the sample cross-sections. According to the requirements of GB/T27552-2011 standard, microhardness values of the weld zone, heat affected zone (HAZ), and base metal zone near the surface of the weld section, as well as the weld zone and base metal zone section along the depth direction were measured via an MHVS-1000Z Vickers hardness tester with a testing force of 10 N and a dwell time of 12 s. After removing the load, four vertices of the indentation were selected to calculate the hardness value, with the distance between adjacent test points of 2 mm. An AGX-300KNV electronic static tensile testing machine was used with a strain rate

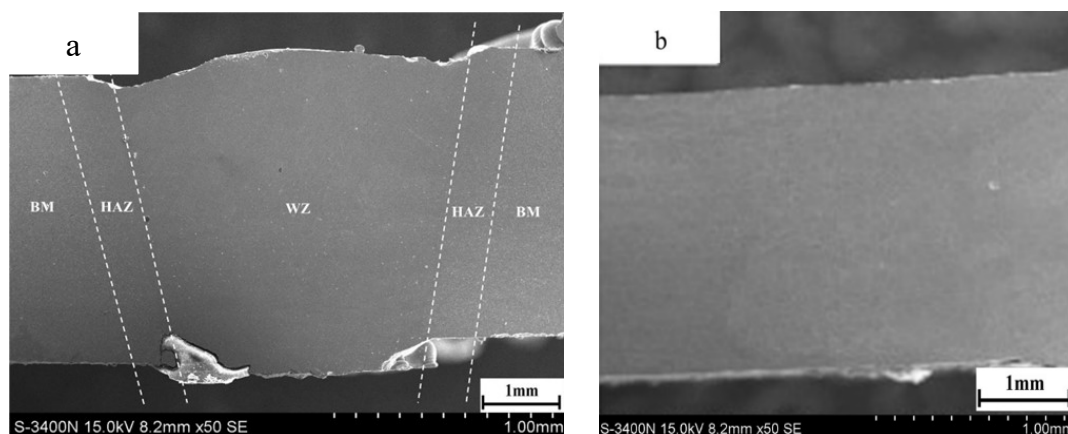


Fig. 2. Cross-sectional morphology of (a) the welded joint and (b) the base metal

of 10^{-2} s^{-1} . The fatigue properties were determined using the TST-D4205L low-cycle fatigue tester using sinusoidal input signals, with a frequency of 10 Hz, stress ratio $R = 0.1$, and a base number of cycles of 10^6 .

3. Results and analysis

3.1. X-ray nondestructive testing

Nondestructive testing for micropores in the welds of samples before and after UIT was performed. The porosity was tested with the Sienz manufacturer's ap53 mm automatic porosity tester and measured with the equal particle size analysis software and programs. Porosity was compared between the welded joints; the results are shown in Fig. 3. Round black spots were visible at the weld toe in the sample without UIT, indicating microporous defects. By contrast, no microporous defects were detected at the welded joints after UIT, indicating that UIT allowed the material surface to absorb the kinetic energy as the tensile stress

field gave way to the compressive one. Secondary fine-grained strengthening occurred, reducing defects on the weld surface, including micropores and cracks. This further improved the quality of laser filler wire welding of the TC4 titanium alloy.

3.2. Phase analysis

The phase composition of the welds before and after UIT is shown in Fig. 4. It can be seen from the XRD spectra that the weld before UIT was primarily composed of the phase and a small amount of the residual β phase. During laser welding, a high heat input coupled with rapid cooling at the weld resulted in a rapid β phase transformation in the solidified titanium alloy [13]. There was hardly time for the α phase to precipitate, while the β phase underwent diffusionless transformation. The β phase was almost completely transformed into the acicular α' martensite phase that shared the same chemical composition as the base metal but had a different crystal structure. The content of the residual β phase was very low. The formation of a large α' martensitic phase in the

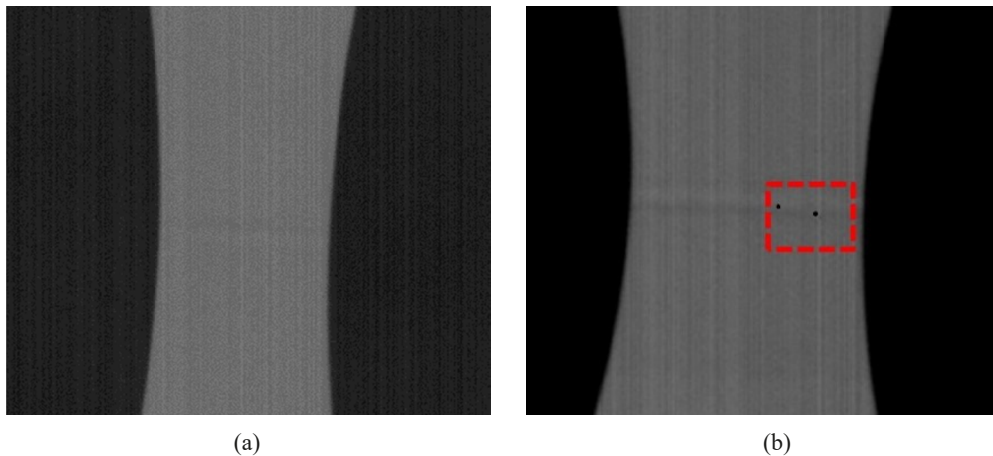


Fig. 3. X-ray nondestructive testing of the welded sample before (a) and after UIT (b)

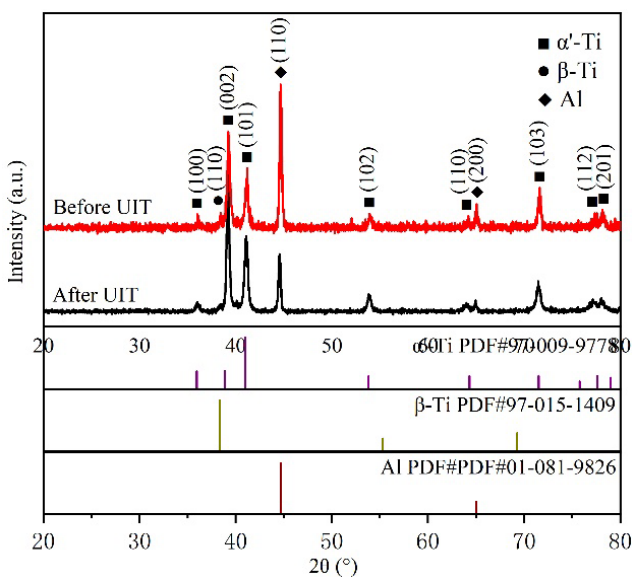


Fig. 4. XRD phase detection spectrum of welds before and after UIT

welded joint increased the microhardness and tensile strength of the welded joint. The phase analysis indicated the same chemical composition of the welds before and after UIT. UIT had no impact on the LFW joint in the TC4 titanium alloy.

3.3. Microstructure examination

The micromorphology of the LFW joints before and after UIT is shown in Fig. 5. It can be known that after UIT, the BM surface was smoother and more tightly structured, and a plastic deformation zone was formed (Fig. 5b). The alloy was refined microstructurally, with the predominance of the primary α phase and lamellar $\alpha+\beta$ phases. In the HAZ, acicular α' martensite phase, granular α phase, and a small amount of the $\alpha+\beta$ phase were observed [14] (Fig. 5d). In the WM, the columnar β crystals grew rapidly. WM was mainly composed of acicular α' martensite phase and granular α phase (Fig.5f). This is because as

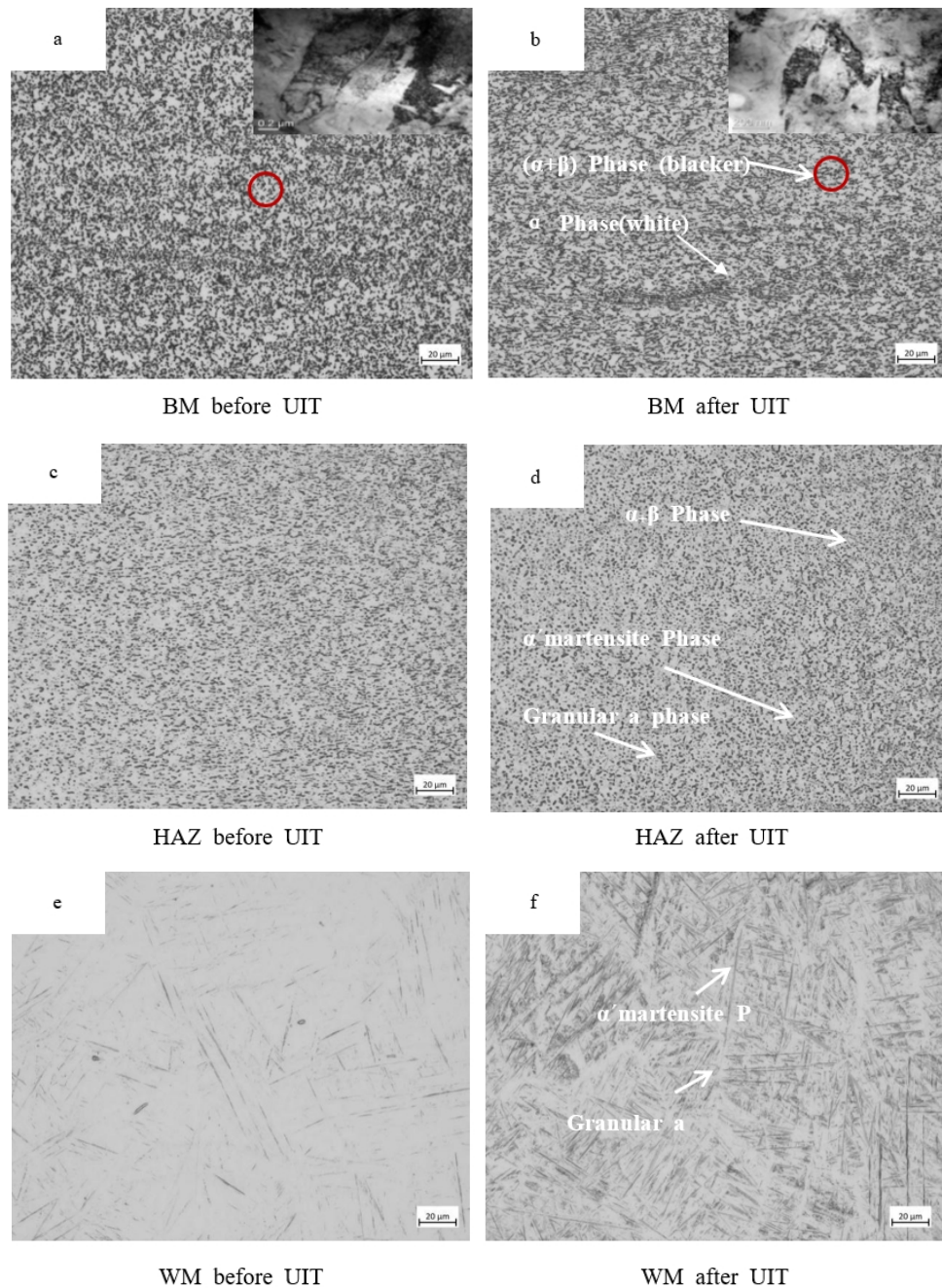


Fig. 5. Microscopic images of the TC4 LFWW: BM zone before (a) and after UIT (b); HAZ before (c) and after UIT (b); WM zone before (d) and after UIT (e)

WM was cooled rapidly, some α phases solubilized at the edge of the β phase and were transformed to fine α' martensite phase. Once the martensite nucleated, the growth was soon completed, which gave rise to the basket-weave structure. This observation agreed with that of Xu et al. [15].

3.4. Performance tests

3.4.1. Microhardness

The microhardness curves of the welded alloy before and after UIT are shown in Fig. 6. Different phases in the TC4 tita-

nium alloy were ranked in descending order of microhardness as follows: α' martensite phase $>$ α phase $>$ β phase [16]. Since the base metal had a higher content of the β phase, it had the lowest average microhardness (350 HV) before UIT. On the contrary, the microhardness of both HAZ and WM (550 HV) was higher than BM's. This is because as the heat input of welding increased, a large amount of the martensite generated in WM facilitated the dissolution of the Al element [17]. Besides, solute gas atoms were generated in the weld pool, and their interactions impeded the fast growth of crystal grains. The fine-grain strengthening was enhanced. After UIT, the microhardness in each zone increased dramatically. The average microhardness values in BM and WM were 442 and 623 HV, respectively, exceeding those

before UIT by 26.3% and 13.2%. The weld microstructure was further refined and deformed due to shock, vibration, and tangential extrusion provided by UIT. Plastic slip occurred, and according to XRD analysis results, a large α' martensite phase with high dislocation density was formed in the weld, inducing a strain-hardening effect and higher microhardness in the weld.

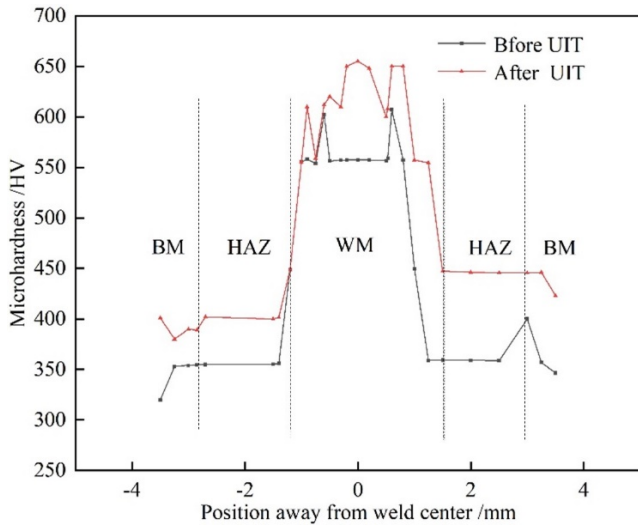


Fig. 6. Microhardness curves of the TC4 LFWW joint before (black line) and after UIT (red line)

3.4.2. Tensile tests

Static load tensile tests of the laser filler wire-welded TC4 joints before and after UIT were performed. The results are shown in Fig. 7. The tensile strength of the welded joint was 775 MPa after UIT vs. 749 MPa base metal, indicating an improvement of 3.4%. The ultrasonic impact refined the weld grains, promoting uniform plastic deformation and small stress concentration when subjected to external force, which improved tensile strength [18].

Fig. 8a shows a rough fracture surface before UIT, with long, thick cracks extending to the material surface. Fig. 8b

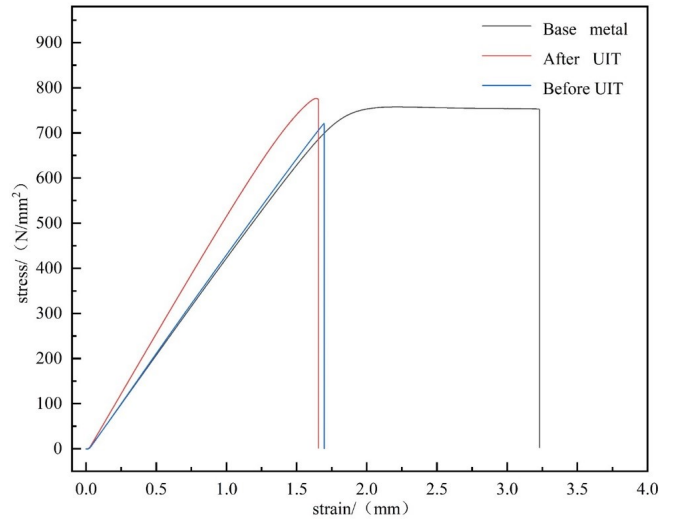
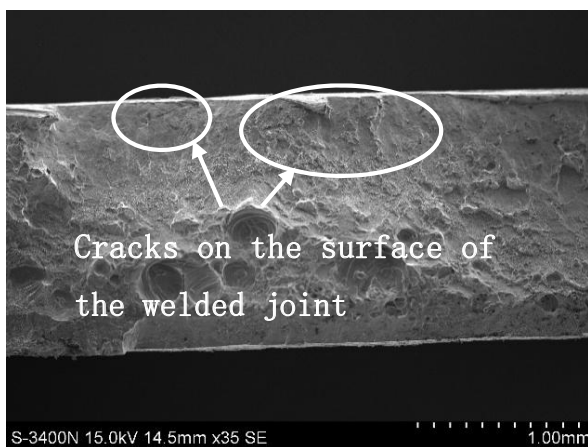


Fig. 7. Tensile curves of the welded samples before and after UIT

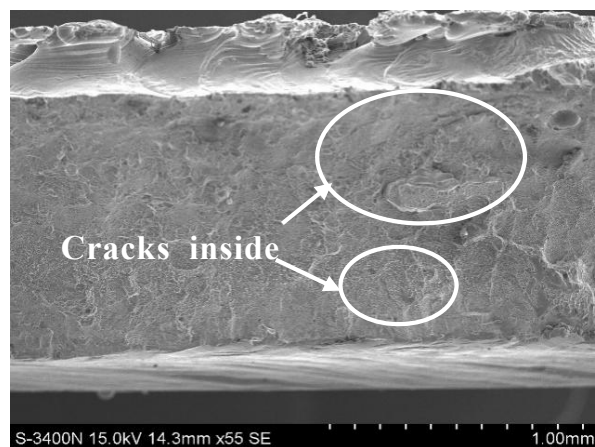
features the fine and smooth fracture surface after UIT, with inward propagating thin cracks. This difference occurred because UIT refined the coarse grains on the material surface and increased material uniformity and consistency, inhibiting crack propagation on the surface. In addition, according to the tensile fracture morphology, the fracture mode of tensile specimens before and after ultrasonic impact was dimple fracture. After the ultrasonic impact, the number of dimples increased, the size of dimples decreased, and the distribution of dimples became more uniform, indicating the improvement of the weld strength by the ultrasonic impact, which complies with the improvement of tensile strength in static tensile tests. UIT also affected the material's inner structure: its grains became more tightly packed, and the cracks only propagated locally.

3.4.3. Fatigue properties

Fig. 9 shows the fatigue curves of the TC4 LFWW joint before (a) and after UIT (b), as well as of the base metal (c).



(a)



(b)

Fig. 8. Tensile fracture morphology of the UIT-treated laser-welded TC4 joint: a) before UIT; b) after UIT

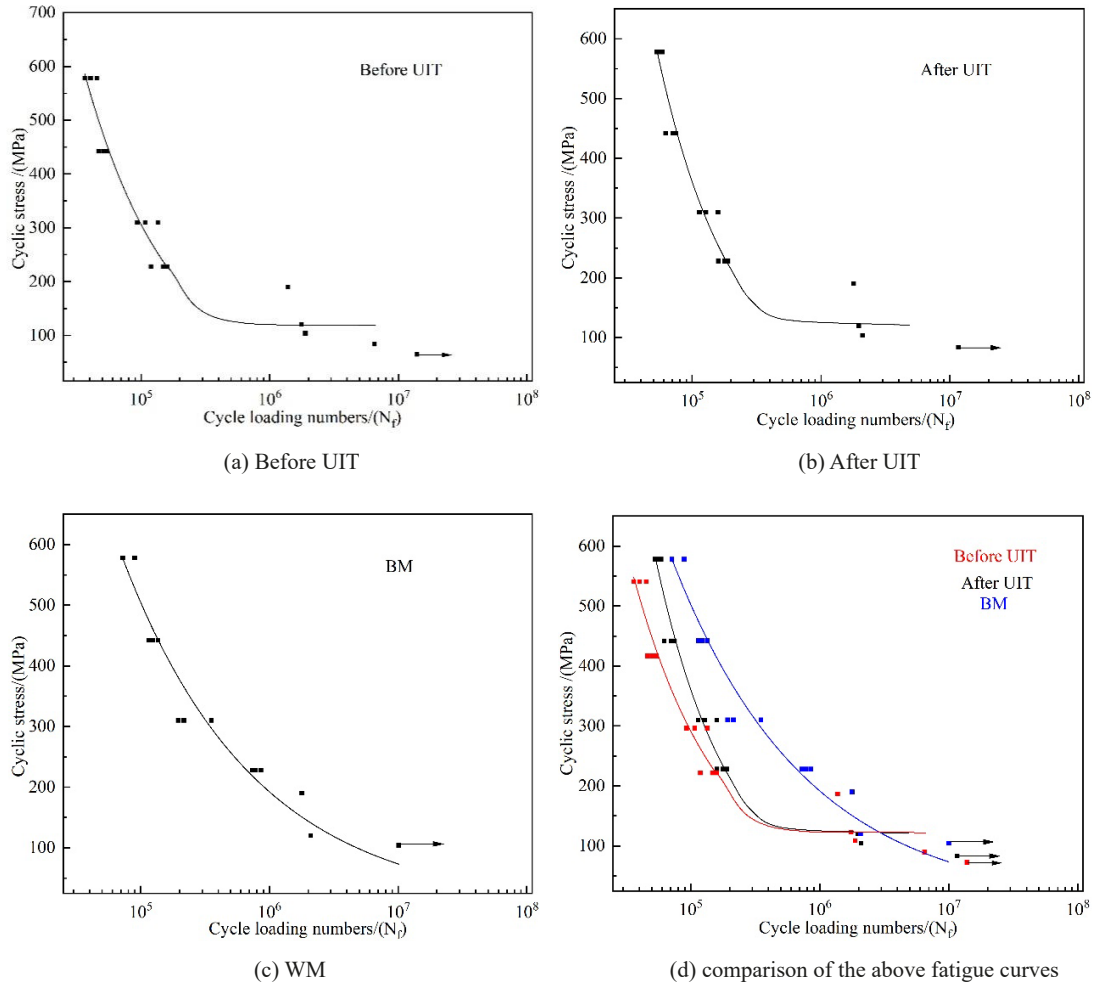


Fig. 9. Fatigue curves of the TC4 LFWW joint: (a) before UIT; (b) after UIT; (c) of the base metal; (d) comparing the above fatigue curves

TABLE 2 and Fig. 9(d) show that after 10^7 cycles of loading, the fatigue samples were not fractured. The corresponding maximum cyclic stress was the fatigue limit of the LFWW joint in the titanium alloy. Besides, the fatigue limits of the base material and the weld before and after UIT were 104, 64.6, and 83.6 MPa, respectively. The fatigue limit of the TC4 LFWW joint increased by 24.4% after UIT compared to that before UIT. The fatigue limit of the welded joint after UIT was 86.6% of the base material's.

TABLE 2

Fatigue test results

Process mode	Cyclic stress	Number of loading cycles		
		1	2	3
Before UIT	578	36517	45432	40425
	442	50875	46645	54335
	104	1846351	1894205	1850657
	64.6	13920735	13923512	12497357
After UIT	578	53126	56642	58825
	442	70873	67345	74675
	104	1964735	2097652	1989253
	83.6	10835324	11623605	11622752
BM	578	72423	89656	90545
	442	135754	123575	115235
	104	10107325	10107325	97535

Fig. 10 shows the fatigue fracture morphology of the TC4 LFWW joint. The cracks originated from the weld surface, and there were multiple sources of cracks.

The above phenomenon can be explained by the surface stress concentration, which promoted crack initiation [19] and further crack propagated toward the weld center by the cleavage and slip mechanisms. The crack propagation zone presented a radial pattern with visible fatigue striations and neat propagation paths. This can be attributed to the formation of slip bands due to dislocation movement in the free surface of the welded alloy under fatigue loading. These slip bands extended and intersected with each other to give rise to radial striations. Fig. 11 shows the fatigue fracture morphology after UIT.

It can be seen from Fig. 11 that the cracks originated deep in the weld, presenting a radial pattern near the air holes, intersecting with each other and pointing toward the site of initiation. This is because the weld became microstructurally denser after UIT and formed a plastic deformation zone. The blocking effects offered by crystal boundaries and grains delayed crack initiation on the surface and reduced the fatigue crack propagation rate. The fatigue band spacing diminished in the fatigue propagation zone. The bands were wavy and perpendicular to the crack propagation direction and finally became striation. Thus, the striation-type fracture occurred. Tang et al. [20] suggested that fatigue band

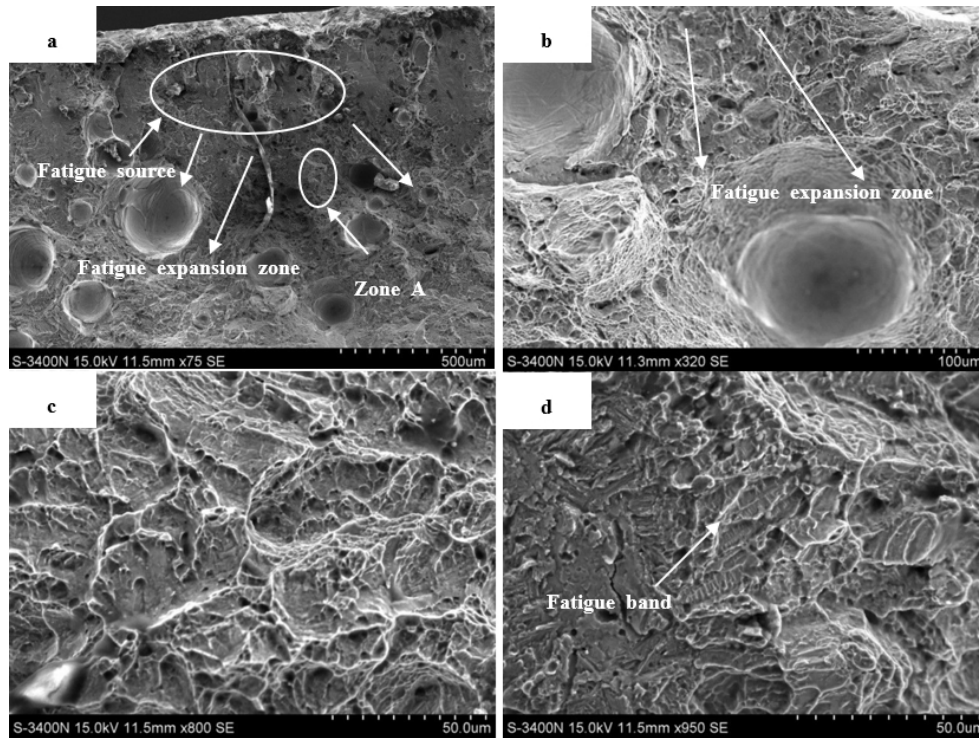


Fig. 10. Fatigue fracture morphology of the TC4 LFWW joint before UIT: (a) overall view of the fracture; (b) crack propagation path; (c) magnified view of the crack propagation path; (d) magnified view of zone A

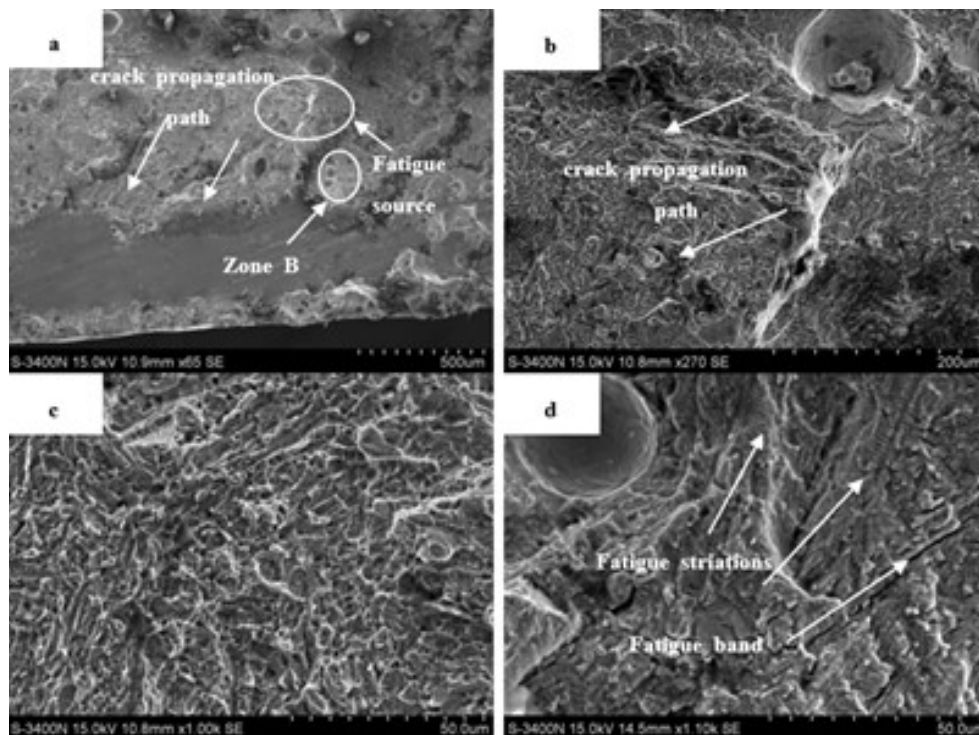


Fig. 11. Fatigue fracture morphology of the TC4 LFWW joint after UIT: (a) overall view of the fracture; (b) crack propagation path; (c) magnified view of the crack propagation path; (d) magnified view of zone B

spacing could be used to approximately characterize the fatigue crack propagation rate. A smaller fatigue band spacing suggested a slower crack propagation. From this conclusion can obtain that the speed of fatigue crack propagation after UIT was lower than before. UIT effectively decreased the fatigue crack propagation

rate, which confirmed the ability of UIT to improve the fatigue properties of the TC4 LFWW joint.

Fig. 12 shows the fatigue fracture morphology in the instantaneous fracture zone before and after UIT. It can be seen that dimples were sparsely distributed in the instantaneous fracture

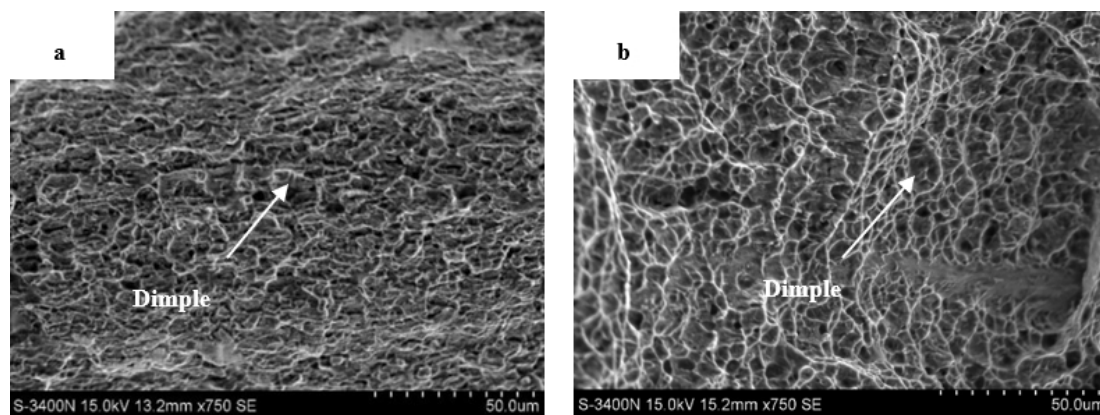


Fig. 12. Fracture morphology of TC4 LFWW joint before (a) and after UIT (b)

zone of the weld without UIT. By contrast, many dimples with increased density and depth were observed in the instantaneous fracture zone in the fatigue fracture after UIT. The UIT-treated welded alloy had better fatigue performance since denser and deeper dimples indicate higher fatigue resistance.

4. Conclusions

- (1) This study used X-ray nondestructive testing (NDT) to detect the porosity defects of welded specimens before and after ultrasonic impact. Black holes and micro-porosity defects were visible at the weld toe of the specimens without ultrasonic impact treatment. After the ultrasonic impact, no obvious defects were detected in the weld seam of the sample, and the high-frequency impact changed the surface stress field of the weld from tensile stress to compressive stress and absorbed kinetic energy. The secondary fine crystal strengthening reduced the defects such as micro-pores and cracks on the weld surface. It improved the quality of laser wire filling welding of TC4 titanium alloy to a certain extent.
- (2) A high cooling rate of the weld resulted in fast β phase transformation in the solidified titanium alloy, and the β phase underwent a diffusionless transformation to give rise to the acicular martensite phase; the β phase is almost completely transformed into acicular α' martensite with the same composition as the base material but different crystal structure. The XRD-based phase analysis indicated the predominance of the α' phase in the weld plus a small amount of the residual β phase after UIT. The formation of a large amount of α' martensitic phase in the welded joint increases the microhardness and tensile strength of the welded joint. The chemical composition of the welds before and after UIT remained constant, indicating that UIT did not alter the phase composition of the LFWW joint in the TC4 titanium alloy. WM and BM shared similar microstructural changes after UIT. The crystal grains were more tightly packed and had more refined microstructure.
- (3) A plastic deformation zone was formed on the joint surface after UIT. The microhardness in each zone increased significantly after UIT. The average microhardness in the weld was 623 HV. After UIT, the average microhardness increased by 26.3% in BM and about 13.2% in WM.
- (4) The tensile strength of the weld treated by high-frequency ultrasonic impact is 775 MPa, the base metal strength is 749 MPa, and the tensile strength is increased by 3.4%. The ultrasonic impact refined the weld grains, and the weld was subjected to uniform plastic deformation, which improved its tensile strength. Before high-frequency ultrasonic impact, the fracture surface was rough, with a long, wide crack extending on the specimen surface. Ductile fracture with dimples was the main fracture mode of tensile specimens before and after ultrasonic impact. After ultrasonic impact, the number of dimples increased, their size decreased, and their distribution became more uniform, indicating weld strength improvement by ultrasonic impact, which was confirmed by the increased tensile strength in static tensile tests.
- (5) Compared with before UIT, the fatigue limit of TC4 titanium alloy LFWW joint after UIT is increased by 24.4%, and the fatigue limit of titanium alloy LFWW joint after UIT is 86.6% of the base material.
- (6) After UIT, the fatigue band spacing decreased, many dimples appeared in the transient fracture area of fatigue fracture after UIT treatment, and the dimple depth and density increased after UIT. Therefore, the weld had a higher fatigue resistance.
- (7) The fatigue crack propagation rate after UIT significantly dropped. The test results confirmed that UIT improved the fatigue properties of the LFWW joint in TC4 titanium alloy.

REFERENCES

- [1] T. Gao, K. Wang, Z. Ling, Z. Wang, Effect of a compound energy field with temperature and ultrasonic vibration on the material properties and bending process of TC2 Titanium alloy. *Materials* **14** (23), 7192(2021).
- [2] T. Yang, Y. Xiao, Y. Zhuang, J. Liu, H. Li, Y. Wang, Effect of microstructural heterogeneity on corrosion fatigue crack growth

- behavior of 60-mm thick-plate TC4 titanium alloy NG-GTAW welded joint. *Int. J. Fatigue* **163**, 107030 (2022).
- [3] Q. Zhao, Q. Sun, S. Xin, Y. Chen, C. Wu, H. Wang, et al., High-strength titanium alloys for aerospace engineering applications: A review on melting-forging process. *Mater. Sci. Eng. A* **845**, 143260 (2022).
- [4] Z. Wang, W. Zhou, K. Luo, H. Lu, J. Lu, Strengthening mechanism in thermomechanical fatigue properties of Ti6Al4V titanium alloy by laser shock peening. *Int. J. Fatigue* **172**, 107631 (2023).
- [5] Y. Liu, T. Wang, H. Chen, Z. Li, S. Li, D. Wang, et al., Impact behaviors of additively manufactured metals and structures: A review. *Int. J. Fatigue* **191**, 104992 (2024).
- [6] X. Liu, Z. Li, Z. Xu, J. Yan, Effect of ultrasonic power on the microstructure and mechanical properties of TC4 alloy ultrasonically brazed joint using Zn filler. *Int. J. Adv. Manuf. Tech.* **119**, 4677-4691 (2022).
- [7] M.M. Quazi, M. Ishak, M.A. Fazal, A. Arslan, S. Rubaiee, A. Qaban, et al., Current research and development status of dissimilar materials laser welding of titanium and its alloys. *Opt. Laser Technol.* **126**, 106090 (2020).
- [8] K.S. James, The influence of sheet conditions on the formability of titanium alloys at room temperature. University of Strathclyde (2021).
- [9] J. Zhang, X. Li, D. Xu, R. Yang, Recent progress in the simulation of microstructure evolution in titanium alloys. *Progress Nat. Sci. Mater. Int.* **29** (3), 295-304 (2019).
- [10] J.Q. Li, R. Michael, B. Frank, Development of a high-frequency test system to study the wear of ultrasonic welding tools. *Metals* **13** (12), 1935 (2023).
- [11] J. Gong, L. Li, S. Meng, R. Huang, J. Zou, H. Cao, Study on stability and microstructure properties of oscillating laser welded 5A06 alloy with narrow gap. *Opt. Laser Technol.* **155**, 108360 (2022).
- [12] A.I. Dekhtyar, B.N. Mordiyuk, D.G. Savvakina, V.I. Bondarchuk, I.V. Moiseeva, N.I. Khripta, Enhanced fatigue behavior of powder metallurgy Ti-6Al-4V alloy by applying ultrasonic impact treatment. *Mater. Sci. Eng. A* **641**, 348-359 (2015).
- [13] Y.H. Zhu, Y.J. Zhang, C.W. Li, J. Zhu, L. Wang, C. Fu, Investigation of microstructure, oxides, cracks, and mechanical properties of Ti-4Al-2V joints prepared using underwater wet laser welding. *Materials* **17** (8), 1778 (2024).
- [14] K. Wang, X.L. Zhao, Z.Y. Cao, Small punch testing of a Ti6Al4V titanium alloy and simulations under different stress triaxialities. *Materials* **17** (17), 4203 (2024).
- [15] S. Xu, M. Han, K. Shen, Y. Cao, A. Fu, C. Ding, H. Tang, Fatigue properties of binary Ti-Ta metal-metal composite with lamellar microstructure. *J. Central South University* **30** (9), 2878-2889 (2023).
- [16] W. Lu, Y. Shi, Y. Lei, X. Li, Effect of electron beam welding on the microstructures and mechanical properties of thick TC4-DT alloy. *Mater. Design* **34**, 509-515 (2012).
- [17] C. Fu, Y. Wang, S. He, C. Zhang, X. Jing, Microstructural characterization and mechanical properties of TIG weld joint made by forged Ti-4Al-2V alloy. *Mater. Sci. Eng. A* **821**, 141604 (2021).
- [18] M. R. Sebdani, H. Bilan, J. Gale, J. Wannan, G. Madireddy, M.P. Sealy, A. Achuthan, Ultrasonic impact treatment (UIT) combined with powder bed fusion (PBF) process for precipitation hardened martensitic steels. *Additive Manuf.* **84**, 104078 (2024).
- [19] K. Shiozawa, Y. Morii, S. Nishino, L. Lu, Subsurface crack initiation and propagation mechanism in high-strength steel in a very high cycle fatigue regime. *Int. J. Fatigue* **28** (11), 1521-1532 (2006).
- [20] D. Tang, X. He, B. Wu, L. Dang, H. Xin, Y. Li, A fatigue life prediction approach for porosity defect-induced failures in directed energy deposited Ti-6Al-4V considering crack growth environment. *Int. J. Fatigue* **184**, 108272 (2024).